GaAs Nanopillar Solar Cell Design on Absorbing Silicon Substrate

Abhejit Rajagopal, Viet Vo, Dingkun Ren, Ramesh B. Laghumavarapu, Diana L. Huffaker

Integrated NanoMaterials Core Laboratory, University of California, Los Angeles 90024
{abhejit, vietvo} @ ucla.edu

Abstract: We present the design of a tandem GaAs-Si solar cell and measure its theoretical efficiency using 3D Finite-Difference Time-Domain (FDTD) electromagnetics solvers. We subsequently test the design's feasibility by aligning the solution to a finite-element (FEM) grid and performing an electrical simulation of the drift-diffusion equations. The combination of these elements is required for prototyping next-generation photonic integrated circuits which may vary in material, dimension, and geometry. Finally, a naive 2^n - point optimization is used to identify geometries with enhanced objectives (photogeneration rates). By comparing the relative photogeneration rates, we conclude such a device will require thick substrates and non-obvious design constraints to achieve current matching and the operation of a tandem cell.

THINGS MISSING:

1. **Fix all citations and references!!!**
2. **Fill in software (Appendix I)**
3. **Write about processing steps and facilities (Appendix II)**
4. **Fix discussion about overall efficiency / conclusion (Results)**
5. **Fix figure for placing the junction (Figure 5)**

Outline

0. Abstract
1. Introduction
2. Solar Cell Design
3. Optical Optimization
4. Electrical Simulation
5. Results
6. Appendix I (Software)
7. Appendix II (Implantation, Fabrication, Growth)
8. References

1 – Introduction

Photovoltaics has made enormous progress in research since the development of advanced nano-synthesis and micro-fabrication tools. The ability to deposit high quality materials with adequate resolution enables the development of revolutionary metamaterials. Nanopillar arrays, for example, exhibit interesting light-coupling properties that make them useful for highly sensitive photodetectors or high-efficiency solar cells. In general, direct-bandgap semiconductors are preferable to those with indirect-bandgap due to the obvious improvement in quantum efficiency. For this reason, expensive III-V semiconductors such as gallium arsenide (GaAs) are preferred over abundant materials such as Silicon (Si), even though their practicality is largely limited to research and specialty applications. In this paper, we explore the design and optimization of monotonically integrated III-V nanopillars on silicon substrates. Made possible by the latest fabrication processes, such a design will maximize solar efficiency and may minimize the average dollar per watt in commercial products.

2 – Solar Cell Design

We inherit the basic design of our solar cell from prior demonstrations of high-efficiency nanopillar arrays [citation]. Following the high-temperature metal-organic chemical vapor deposition (MOCVD) process[Appendix I] to grow III-V nanopillar arrays, wafers are typically coated with transparent polymers and conductive oxides to serve as large-area contacts for collecting generated carriers. Previously[citation], *Mariani et al* has shown that these transparent materials have the ability to concentrate optical modes, effectively lensing light into the nanopillar unit cell. More than the concentrators, nanopillar arrays themselves exhibit dramatically lower reflectance due to the increased surface area and effective “light trapping” in such devices. **Figure 1** shows the structural cell design.

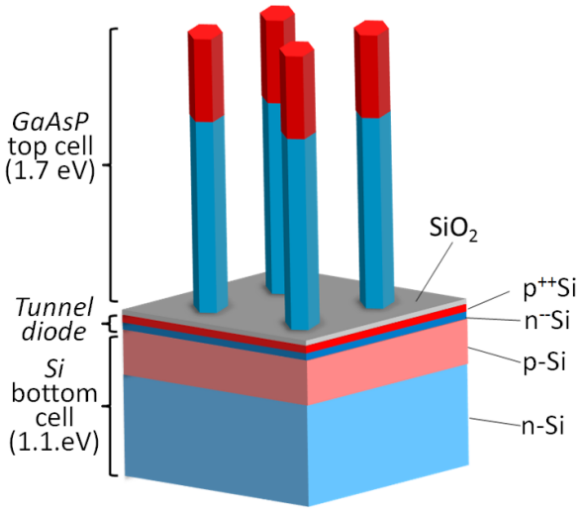
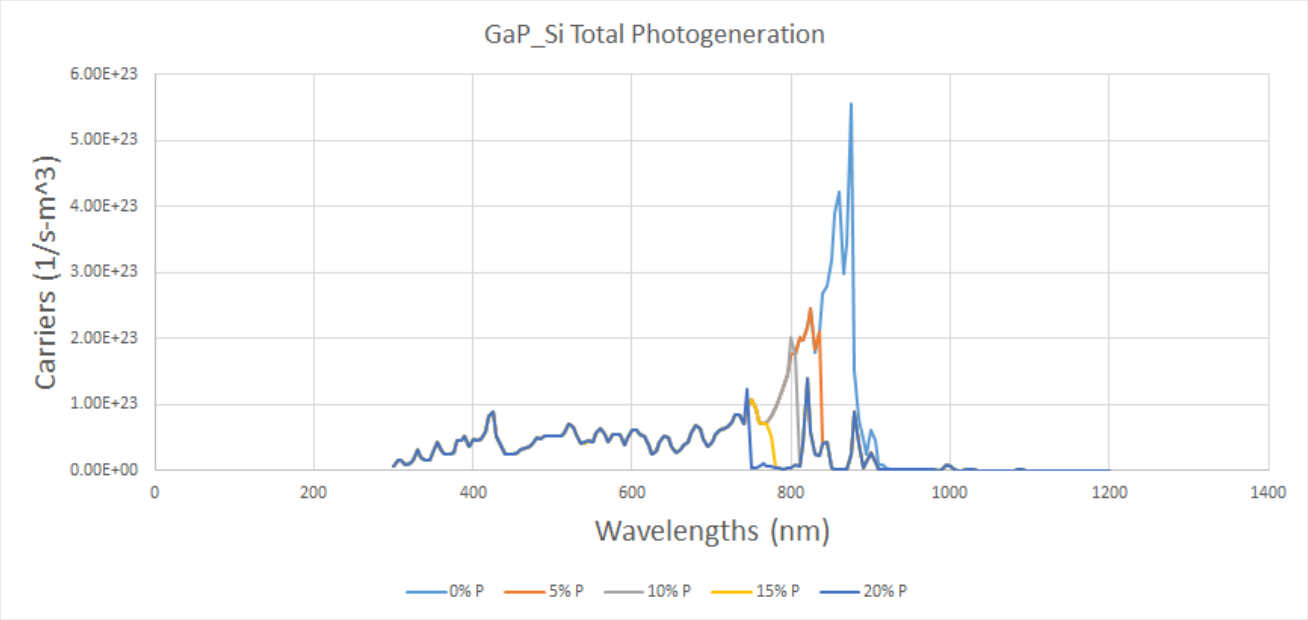


Figure 1: Proposed tandem solar cell design: *GaAs(P) nanopillar arrays on Silicon substrate.*

In our initial design, we consider uniform arrays of GaAs(P) nanopillars grown on Si substrate on the order of 1e2 nm due to demonstrated improvements in cell efficiency [citation] [citation] in this regime. By including silicon as the absorbing substrate, we aim to capture a larger area of the solar radiation spectrum and improve overall cell efficiency. By 3D

FDTD simulation, we found that phosphorus (P) incorporation reduced the overall efficiency of these devices because of the substrate contribution is not enough to counter the loss in photon absorption due to the increase in the bandgap between GaAs and GaAs(P) at various incorporation levels. This postulate was tested by simulating various optimized structures and tracking the relative contributions of the substrate and pillar cells. The results of the most optimized structure is shown below in **Figure 2**.



Phosphorus %	Total PG (1/s-m^3)
0	9.94E+24
5	6.95E+24
10	6.01E+24
15	5.15E+24
20	4.75E+24

Figure 2: *GaAs(P) nanopillar arrays on Silicon substrate have substantially lower photogeneration rates as compared to identical GaAs structures.*

3 – Optical Optimization

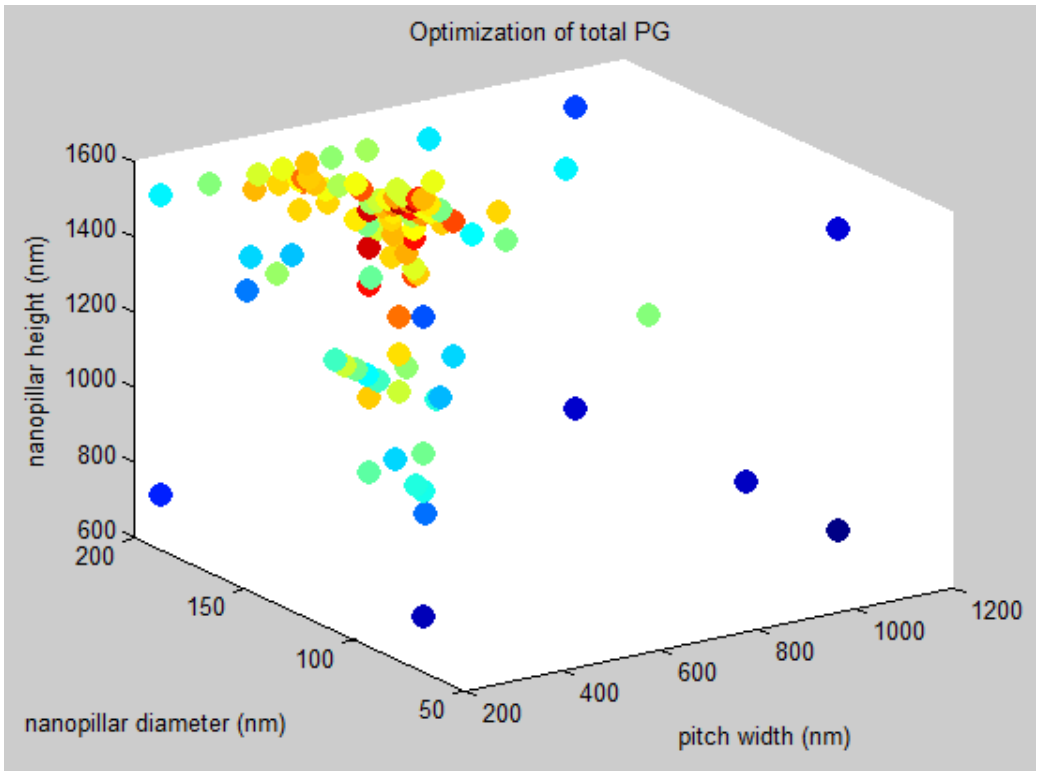
While particular geometries are known to increase the absorption and overall efficiency of solar junctions, these solutions are not necessarily obvious due to intricacies in the subwavelength regime. In order to select an appropriate mask layout, we employed Lumerical's Finite-Difference Time-Domain (FDTD) wave solver to determine the fields

incident on nanopillar arrays of various cell geometries. Our goal was to optimize the photogeneration of the these nanopillar structures by varying three structural parameters: pillar diameter ranging from 80 nm to 200 nm, pillar height ranging from 700 nm to 1500 nm, and pitch width ranging from 250 nm to 1100 nm. Each simulated structure would be swept through a range of monochromatic light with wavelengths between 300 nm and 1200 nm. To begin, we created a script on Lumerical which generalized the nanopillar structure, allowing us to freely vary the dimensions of the three structural parameters, as well as the material, the source, and any of the FDTD settings.

In the script, we defined the FDTD simulation region with periodic and symmetric boundaries in the x and y directions respectively, and PML boundaries for the z direction. The bottom of the structure consisted of a silicon (Si) layer 500 nm high, followed by a layer of glass (SiO2) 50 nm high. A benzocyclobutene (BCB) layer was then added above the SiO2 with a height that varied linearly with the pillar height. Subsequently, an indium tin oxide (ITO) layer 50 nm high was added above the BCB. A hexagonal GaAs pillar was inserted in the center of the structure above the Si substrate, going through the SiO2, BCB, and ITO. Finally, the top of the pillar was placed inside an ITO hemispherical cap that had a 250 nm diameter in the x-y direction. Both the pillar and the substrate had a mesh of 15 nm in dx, dy, and dz.

Lumerical FDTD, as opposed to some other implementations, is known to have some difficulty with broadband simulations. Instead of using discrete *n* and *k* values for each material, Lumerical uses a smooth estimated curve of the values that helps to preserve its solutions. This caused many of the GaAs *k* values to be nonzero after the band gap, thus creating a false report of photogeneration in the simulation. To solve this issue, we used the generalization script to generate structures each varying only in the source wavelength. We varied the wavelengths of each of the structures in 5 nm increments from a range of 300 nm to 1200 nm, totaling in 181 structures. By running each structure under a monochromatic light source, we were able to bypass Lumerical's FDTD estimated material model data, and instead use the sampled material data directly [citation]. The script automatically collected the data for each of the 181 simulations, normalized it with respect to the structure's volume, and returned the results in a CSV file. This data was finally normalized with the AM1.5 Spectrum, although alternate re-normalizations are possible. Our new results no longer had photogeneration after the band gap, which agrees with the expected physics. We used this procedure for all of our future simulations.

In order to find an optimized structure, we performed an 8-point optimization by annotating the 8 corner cases based on the maximum and minimums of the pitch width, pillar height, and pillar diameter. A Matlab code was created to see which corner case produced the highest photogeneration and to compare different distributions, such as before and after spectrum normalizations or parameter manipulations. The 8-point optimization is shown in **Figure 3a.** One relationship we discovered was that as pillar height decreased, so does photogeneration. Therefore, we focused much of our efforts on varying pitch width and pillar diameter, keeping the pillar height at a maximum of 1500 nm. As we searched through the large parameter space, we identified local maxima and executed over 100 simulations around the area to find the most optimized structure. The optimized structure is shown in **Figure 3b** and its graph of photogeneration vs. wavelength is shown in **Figure 3c**.


Optimization of total PG
nanopillar height (nm)
1600
1400
1200
1000
800
600
200
150
100
50
nanopillar diameter (nm)
200
400
600
800
1000
1200
pitch width (nm)

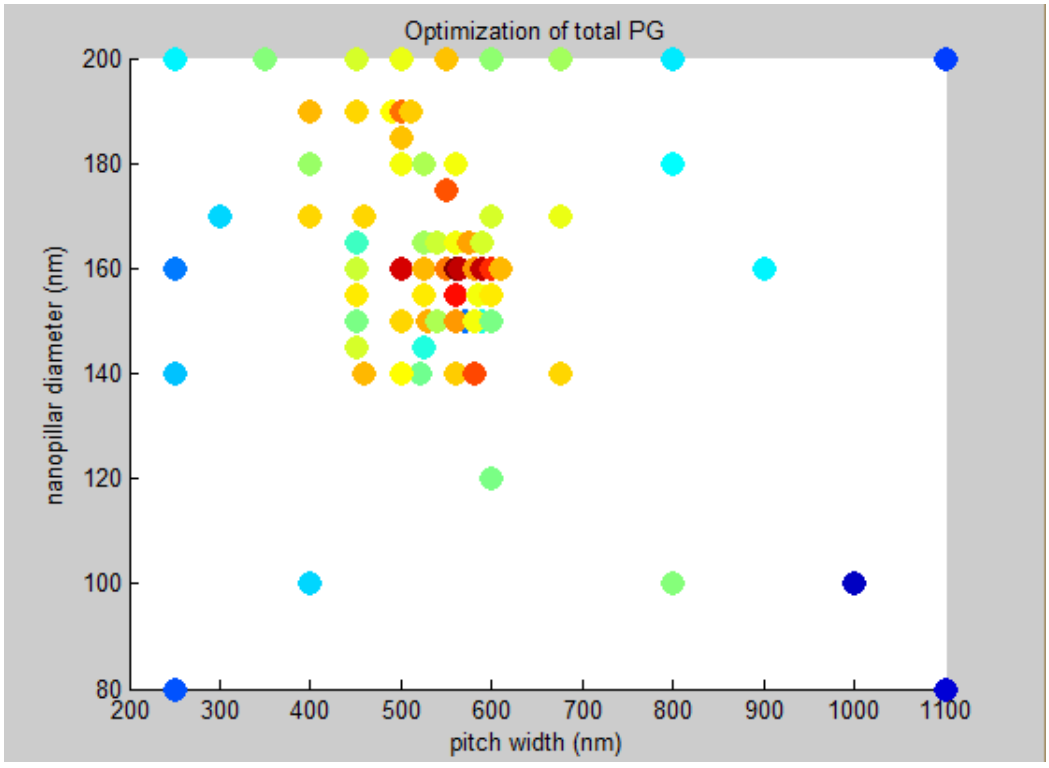

Optimization of total PG
nanopillar diameter (nm)
200
180
160
140
120
100
80
200
300
400
500
600
700
800
900
1000
1100
pitch width (nm)

Figure 3a: *The 8-point optimization gives a good estimation of the structure with the highest photogeneration indicated by the brown points. The optimal structure had a 560 nm pitch width, a 160 nm pillar diameter, and a 1500 nm pillar height.*

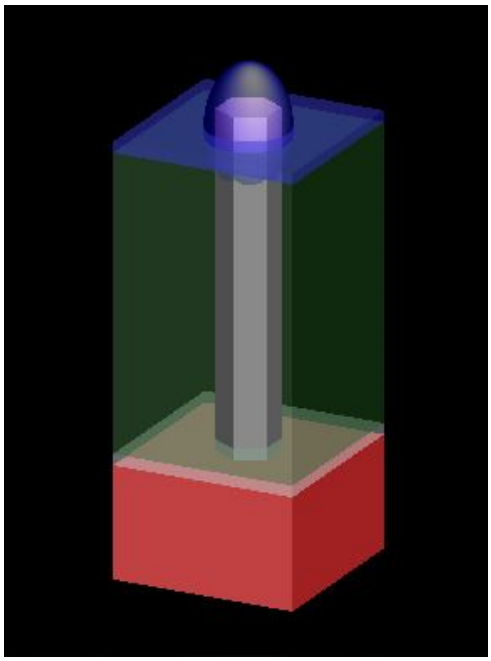


Figure 3b: *Optimized structure having a 560 nm pitch width, a 160 nm pillar diameter, and a 1500 nm pillar height. From bottom up, structure consists of Si substrate (Red), SiO2 (transparent), BCB (green), GaAs pillar (gray), ITO layer and cap (blue).*

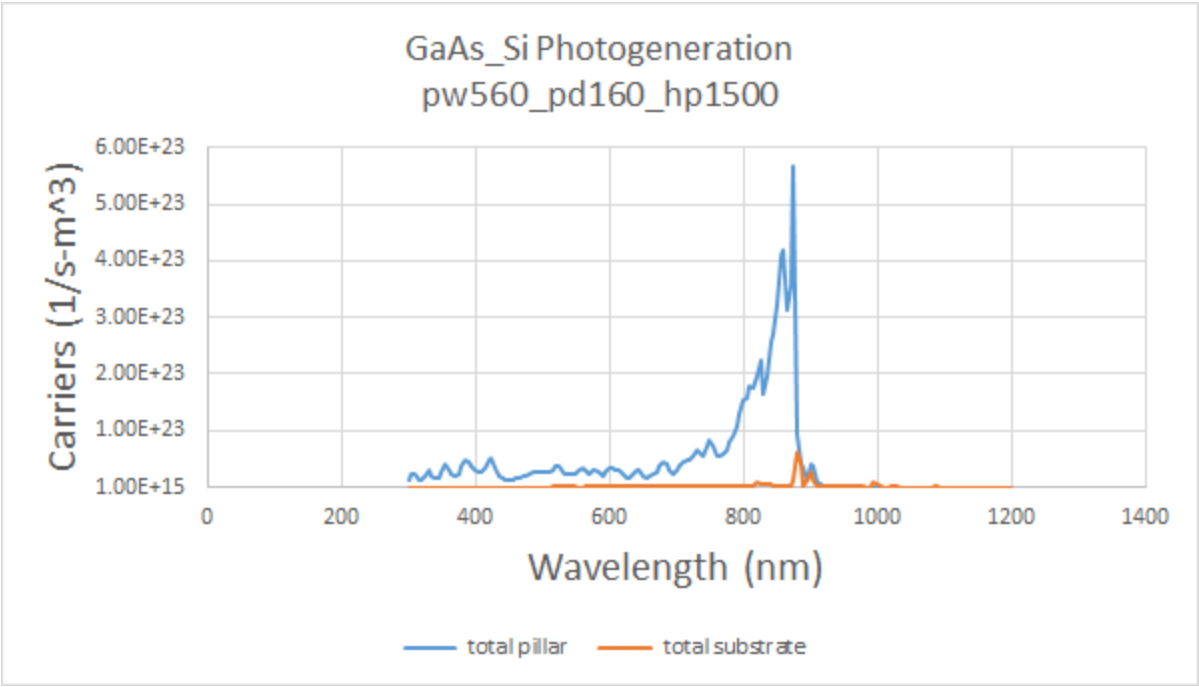


Figure 3c: *Photogeneration of the optimized structure, reaching a peak before the estimated band gap of 890 nm and dieing off after this point.*

4 – Electrical Simulation

By performing a 3D interpolation (interp3D) [github.com/sirgogo/TheAwesomeSimulator/], we map carrier generation rates to a Finite-Element Mesh (FEM) in order to simulate the drift-diffusion process in simple PN junctions. The electrical design, as opposed to the optical design, involves only the metallurgical junctions between p-doped GaAs, n-doped GaAs, and n-doped Si. The transparent conducting oxide (ITO) and polymer (BCB) do not directly contact the device due to an applied surface passivation on the pillar with GaP or AlGaAs and on the substrate with SiO2. The basic electrical device geometry is shown in **Figure 4**.

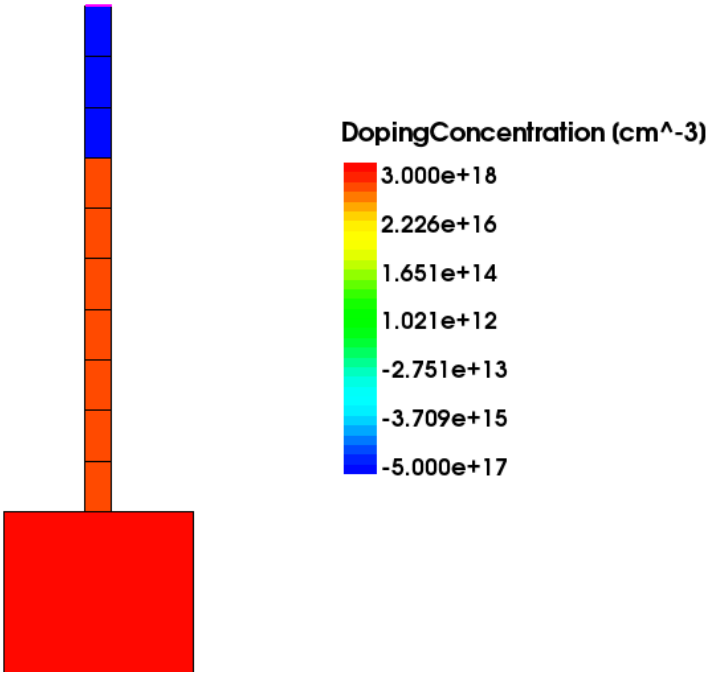
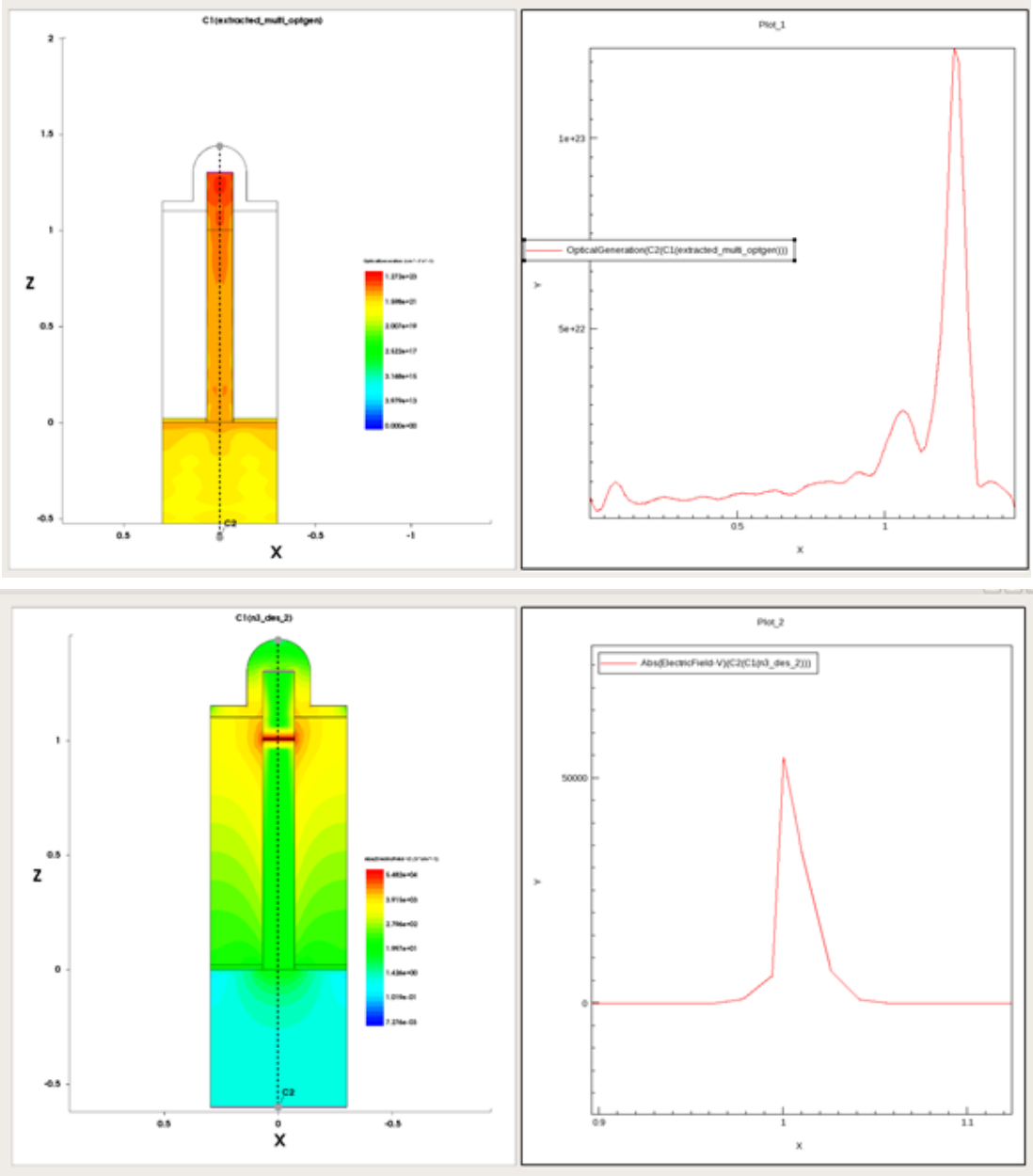


Figure 4: *Basic monolithic III-V nanopillar on Si solar cell device geometry.*

It is worth noting the arbitrary placement of the junction location and doping concentrations. Part of the electrical design requires the optimization of the short-circuit current and open-circuit voltage. By varying the physical junction location, for example, we can modulate the number of carriers swept by the solar-cell. This design concept is similar to that presented in the NOADD photodetector design [citation], in that the location of the photo-generated carriers is important and affects the electrodynamics of device operation. Specifically, by placing the semiconductor junction in the vicinity of concentrated photogeneration regions, more carriers will be swept and the short-circuit current of the

nanopillar cell will increase. **Figure 5** demonstrates how designers may select an appropriate junction position, by coupling the optical and electrical simulations and tracking relative improvements in efficiency.



p-doped axial length (nm)	Jsc (mA/cm^2)
300	~ 4.04
250	~ 4.35
200	~ 4.69
150	~ 4.96
100	~ 5.35

50	~ 5.49

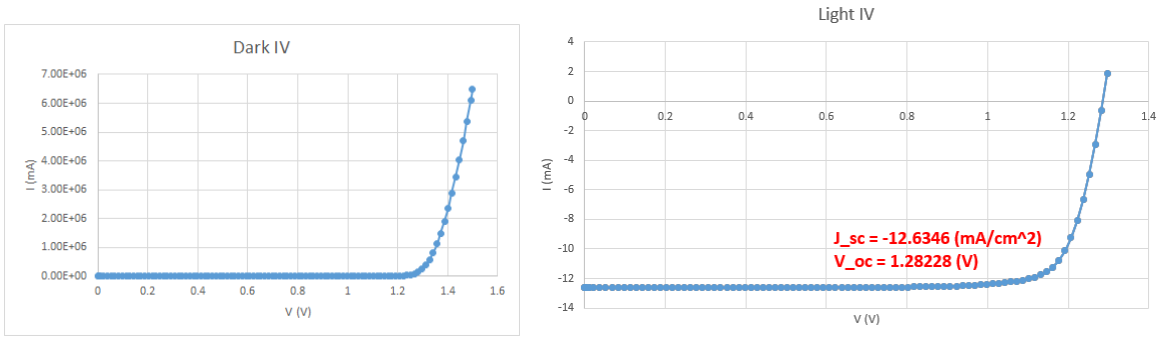
Figure 5: *Placing the semiconductor junction close to the region of maximum photogeneration in the nanopillar results in higher short-circuit currents (Jsc). The high electric field sweeps more carriers and improves the overall efficiency of the solar cell. This is shown via simulation.*

Furthermore, our device architecture is limited by the optical absorption in both nanopillar and substrate. Although III-V nanopillars on Si will be cheaper than conventional III-V arrays, the ultimate solution would be to have two solar cells operating independently (one junction in the pillar, one junction in the substrate). However, per our optical optimization, we determined that the efficiency of the silicon substrate substantially undermines the operation of a III-V nanopillar device. Moreover, the widening of the absorbed spectrum is not dramatic enough to justify the integration of a multi-junction tandem solar cell, since the overall device current will be limited by the highly inefficient cell in the substrate. Finally, we propose the growth of GaAs nanowires on Si as a cost-effective alternative to III-V nanopillar arrays on alternate expensive substrates.

5 – Results

The structure with the highest volume and spectral photogeneration rates was selected as the design candidate. It is worth noting that our optimization did not look at carrier dynamics; here it is assumed that generated carriers will eventually drift across the boundary, and that location does not matter. Obviously, the location does matter in these sensitive devices, as demonstrated in the NOAD design, but the degradative effects in solar cells are usually measured as reductions in external quantum efficiency, as opposed to distortions in sensitive signals, so our initially harsh optimization is generally valid. Our optimized design of 560nm pitch width, 160nm pillar diameter, and 1500nm pillar height produced a stunning *Jsc* of 12.6 mA/cm^2 and *Voc* of 1.28 volts, placing the unit-cell efficiency between 1.1% and 1.6% (for fill-factors of 0.7 and 1.0 respectively). Effectively, the array will have greater efficiency since thousands of such unit cells are contacted in parallel. The simulated I-V characteristics are shown in **Figure 7a.** Further, we can converge these numbers to realistic estimates by measuring devices and matching expected parameters such as the surface recombination velocity, carrier lifetime, and even effective doping concentrations. The parameter space is large, which is why devices must be first designed using theoretical parameters. Using calibrations from GaAsP on GaAs nanowires[citation], we determined a **theoretical efficiency of ___ %**, shown in **Figure 7b**.

A



B

Figure 7: *Light and Dark I-V characteristics for (a) theoretical parameters, and (b) calibrated parameters.*

6 – Appendix I (Software)

In this project, we employed:

-- Lumerical FDTD (finite-difference time-domain) engine for the 3D wave solution

-- Synopsys Sentaurus solver for 3D drift-diffusion equations

-- The open-source AwSimLib (AwesomeSimulation Library) for grids and analysis

In addition, we developed a range of scripts in Matlab and Python to automate the workflow. The most integral of these scripts are summarized below:

--

--

--

-- interp3D

7 – Appendix II (Implantation, Fabrication, Growth)